journal

J. Am. Ceram. Soc., 73 [7] 1936–40 (1990)

Delamination Cracking in a Laminated Ceramic-Matrix Composite

Orfeo Sbaizero,* Panos G. Charalambides,*,* and Anthony G. Evans*

Materials Department, College of Engineering, University of California, Santa Barbara, California 93106

Delamination crack propagation has been investigated in a laminated fiber-reinforced ceramic-matrix composite. The crack growth initiation resistance has been shown to be dominated by the critical strain energy release rate for the matrix. However, the resistance increases with crack extension because of bridging effects associated with intact fibers and, in some cases, intact segments of matrix. The delamination cracks also assume a steady-state trajectory within a 0° layer close to the 0°/90° interface. [Key words: composites, mechanical properties, cracks, laminates, matrix.]

I. Introduction

CERAMIC-MATRIX composites reinforced with aligned fibers that exhibit high "toughness" in tensile (mode I) loading are often susceptible to delamination (mixed-mode) cracking.[1,2] Such cracking, typically encountered in the presence of notches, is also evident in polymer-matrix composites,[3] and in wood.[4] The delamination crack nucleates near the base of the notch and propagates axially outward as the load is increased, causing the material to be notch insensitive.[2,3] The intention of this study is to investigate the resistance of a laminated ceramic-matrix composite to this mode of crack propagation. The problem is not only of fundamental interest, but also of significant technical importance. The presence and growth of delamination cracks in composite laminates may lead to severe reliability and safety problems, such as the reduction of structural stiffness and exposure of the interior to an adverse environment.

The mechanics basis for the study involves analysis of the energy release rates $\mathcal{G}$ associated with the observed delamination morphologies.[4,5] The product of the study is a characterization of the delamination fracture resistance $\mathcal{G}_R$, which provides the basis for a microstructure-based model which relates $\mathcal{G}_R$ to the properties of the matrix, interfaces, and fibers. Such characteristics provide the principles needed to predict relative tendencies for composites to exhibit either mode I matrix cracking or mixed-mode delamination cracking and thus establish a framework for design criteria.

II. Mechanics Summary

The basic mechanics needed to interpret measurements of delamination crack growth have been derived elsewhere.[5–7] The results applicable to the present experiments are briefly summarized in this section. The experiments utilize test specimens (Fig. 1) in which the notch depth w exceeds the laminate thickness and is about one-third to one-half the specimen thickness, h. For this geometry, tested in four-point flexure, delamination cracks are subject to steady-state conditions,[7] provided that the cracks are between the inner load lines and larger than $\sim(1/2)w$.† Linear elastic steady-state stress intensity factor solutions for anisotropic beams have been derived[5] and provide the basis for solutions applicable to laminates.[6] The laminate results have the form

$$\mathcal{G}\frac{(1+\lambda)B^2h^3}{2b_{11}P^2\ell^2} = F(\lambda, w/h, n) \tag{1}$$

where $\mathcal{G}$ is the energy release rate, P is the load, ℓ is the moment arm (Fig. 1), B is the beam width, $2n$ is the number of layers in the symmetric laminate beam, b_{ij} $(i, j = 1, 2)$ are the plane strain elastic compliance constants of the laminae,[5,6] and $\lambda = b_{11}/b_{22}$ is the ratio of the elastic compliance constants in the principal 11 and 22 (Fig. 2(A)) directions. For example, in a fiber-reinforced lamina (Fig. 2(A)), the constants b_{11} and b_{22} are obtained in terms of the elastic properties of the fiber and the matrix, such that for plane strain

$$b_{11} = \frac{1}{E_1}\left(1 - \nu_{12}^2\frac{E_2}{E_1}\right)$$

$$b_{22} = \frac{1}{E_2}(1 - \nu_{23}^2) \tag{2}$$

where

$$E_1 = (\Lambda f + 1 - f)\bar{E}_m \qquad E_2 = \frac{1 + 2\eta f}{1 - \eta f}\bar{E}_m$$

$$\nu_{12} = f\nu_f + (1 - f)\nu_m \qquad \nu_{23} = \frac{1 + 2\eta f}{1 - \eta f}\nu_m$$

$$G_{12} = \frac{1 + 2\eta f}{1 - \eta f}G_m \qquad \eta = \frac{\Lambda - 2}{\Lambda + 2} \tag{3}$$

In the above expressions, E and ν refer to the elastic modulus and Poisson's ratio, respectively, the subscripts f and m denote quantities for the fiber and the matrix within a single lamina, and indices 1, 2, and 3 denote the principal composite directions as shown schematically in Fig. 2(A). Also, in the preceding expressions, $\bar{E} = E/(1 - \nu^2)$ is the plane strain elastic modulus, $\Lambda = \bar{E}_f/\bar{E}_m$, and f is the fiber volume fraction within the laminae.

Trends in the nondimensional function F in terms of the number of layers n, the compliance constant ratio λ, and normalized notch depth $w/(h - w)$ are shown in Figs. 3(A) and (B). As indicated schematically in the above figures, the results obtained from Eq. (1) can be used in the case of symmetric laminates with an arbitrary number of layers $2n$. However, when the beam is composed of a sufficiently large number of layers $(n > 10)$, the corresponding results shown in Figs. 3(A) and (B) can be used even in the case of a general nonsymmetric laminated beam.[6] In such a case, the laminate can be

D. Green—contributing editor

Manuscript No. 198608. Received February 20, 1989; approved February 28, 1990.

*Member, American Ceramic Society.

*Current address: Department of Mechanical Engineering and Engineering Mechanics, Michigan Technological University, Houghton, MI 49931.

†The strain energy release rate is independent of crack length in the steady-state regime, as previously established for bimaterial beams (Ref. 7).

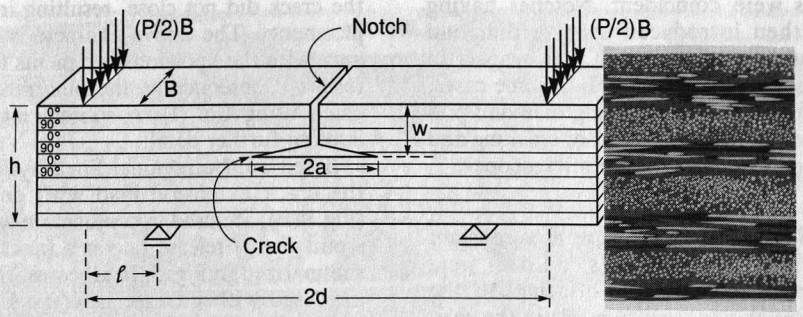

Fig. 1. Schematic drawing of the test specimen and an optical micrograph of the laminate.

treated as a homogeneous orthotropic beam with its longitudinal modulus obtained via the rule of mixtures.[6] The analysis behind Eq. (1) is based on bending theory solutions for heterogeneous beams and accounts for material heterogeneities within the laminae and laminate. Thus, in the analysis, cross sections of the laminated beam are assumed to remain plane after deformation and the stresses carried by each constituent are assumed to be uniaxial and consistent with the bending theory of composite beams. As an additional benefit of this approach, the effective composite properties in the direction of the axial stress are obtained in terms of the number of layers n as a part of the solution. Thus, homogenization criteria regarding n can be established, as discussed elsewhere.[6]

III. Experimental Procedure

(1) Materials

The primary material selected for investigation consists of a 0°/90° cross-ply laminated LAS-II matrix reinforced with SiC Nicalon fibers, prepared by hot-pressing and supplied by United Technologies Research Center.[1,2] The fiber volume fraction is ~0.44. The material has a thin C layer between fiber and matrix which allows debonding and sliding[8,9] and thus imparts high tensile "toughness."[2] This material is also subject to residual strain caused by thermal expansion mismatch, such that the radial stress at the interface is tensile.[9] In some cases, this tensile stress causes thermal interfacial debonding.[9]

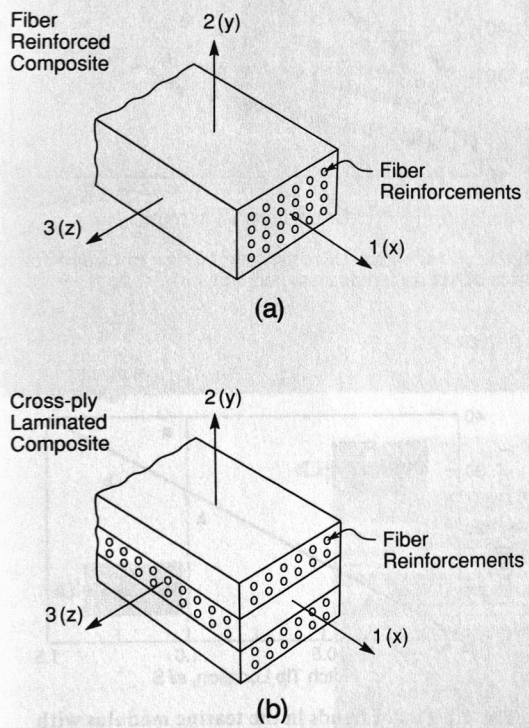

Fig. 2. Orthotropic material directions in (a) fiber-reinforced composite lamina and (b) cross-ply laminate.

(2) Test Specimens

Flexural specimens having dimensions 3 mm × 3 mm × 35 mm were machined from hot-pressed plates such that the

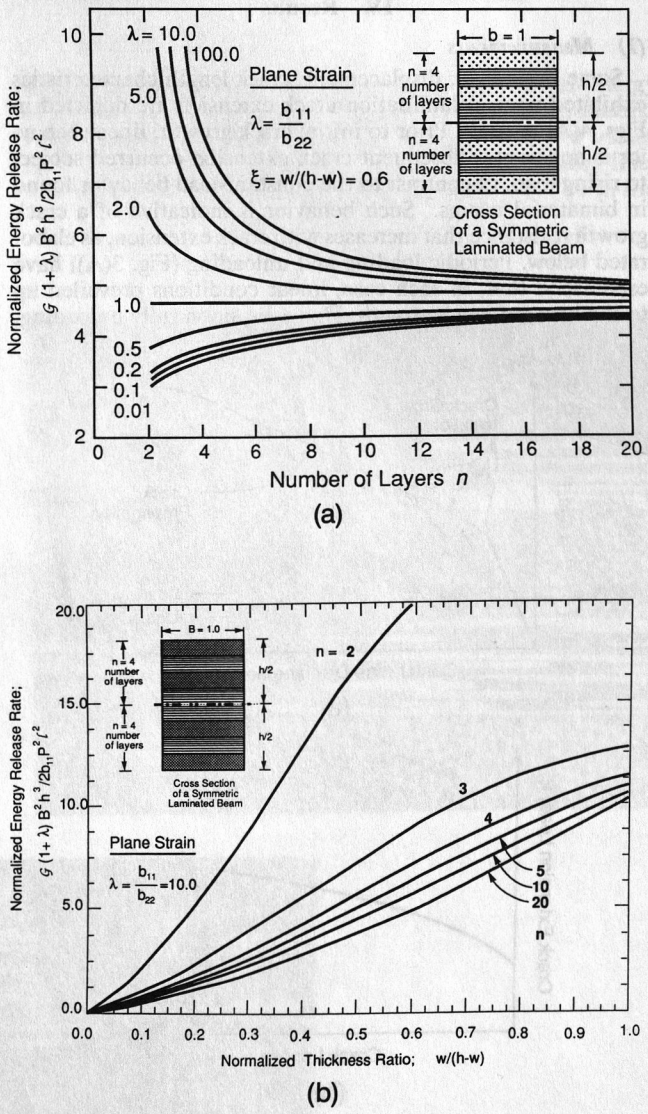

Fig. 3. Trends in the steady-state strain energy release rate $\mathcal{G}$ normalized by the rule of mixtures modulus for the laminate $E_1 = (1 + \lambda)/2b_{11}$: (a) effect of the number of layers in a symmetric laminated beam; (b) effect of notch depth $w/(h - w)$.

fiber and specimen axes were coincident. Notches having widths ≈0.9 mm were then introduced using a diamond blade. The location of the base of the notch with respect to the lamination layer was systematically varied. In some cases, the side surfaces were carefully polished, using diamond polishing media, as needed to make observations of cracking and damage in the optical and scanning electron microscopes.

(3) Test Procedures

Specimens were loaded in four-point flexure at a constant load point displacement rate of $\sim 10\ \mu m \cdot s^{-1}$. Loads were monitored and a displacement transducer attached to the specimen adjacent to the notch was used to measure the relative vertical center line displacement, u.[7] Friction was minimized by emplacing a thin layer of solid lubricant between the specimen and the loading points. Crack lengths were also observed and monitored using a long focal length optical microscope.

Specimens were mostly subject to monotonic displacement rates, resulting in continuous crack extension. In some cases, periodic unloading was performed in order to measure the compliance and to examine the applicability of the linear analysis represented by Eq. (1). Crack lengths were also measured in optical and scanning electron microscopes.

IV. Results

(1) Measurements

Some basic load, displacement, crack length characteristics exhibited upon delamination crack extension are depicted in Figs. 4(A) and (B). Prior to initial crack growth, linear behavior is apparent. Subsequent crack extension occurred subject to rising load, in contrast to the constant-load behavior found in bimaterial beams.[7] Such behavior is indicative of a crack growth resistance that increases with crack extension, as elaborated below. Periodic loading and unloading (Fig. 3(A)) have established that, in each case, linear conditions prevailed up to the onset of crack growth. However, upon fully unloading, the crack did not close, resulting in residual center line displacments. The above characteristics are in broad accordance with the known requirements for the use of linear elastic results. Consequently, the preliminary data analysis is indicated using Eq. (1). A subsequent study will examine this issue in further detail.

Based on the nominal linearity of the behavior, trends in the crack extension load with delamination crack length (Fig. 4(B)) are used in conjunction with Eq. (1) to evaluate the strain energy release rate as a function of crack extension, as summarized in Fig. 5. In all cases, the fracture resistance, $\mathcal{G}_R$, increased with increase in crack length, a, but is always of order 15 to 20 $J \cdot m^{-2}$ at crack growth initiation from the notch ($a \to 0$). The slope (tearing modulus), $T = d\mathcal{G}_R/da$, varied appreciably between specimens, but had a systematic dependence on the location of the notch tip. Specifically, T increased as the distance s between the notch tip and the bottom of the next 90° layer increased (Fig. 6). Furthermore, the results that give the largest T refer to cases in which the notch tip is located in a 0° layer, resulting in a bridge of intact material at the crack center (see Fig. 8(C)).

(2) Observations

Crack path observations (Figs. 7 and 8) indicate that the crack always attains a steady-state trajectory when the crack length $a \gtrsim w/2$. This trajectory coincides with a plane just within and near the base of the 90° layer next to the notch tip (Fig. 8). This plane is seemingly selected by the crack whatever the original location of the notch tip (Fig. 7). Such behavior is exemplified in Fig. 7(B) by a crack which emanates from a notch tip located at the upper interface of a 90° laminate layer. It is evident that the crack initially progressed to-

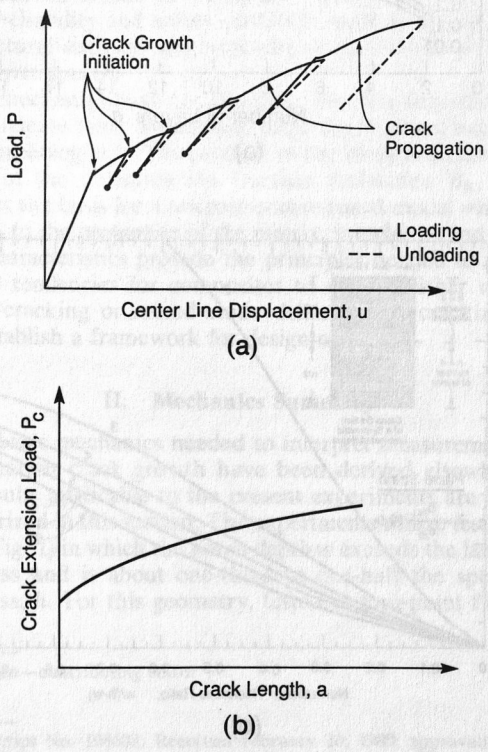

Fig. 4. Loading curves obtained during testing: (a) Load–displacement curves showing the crack extension region; (b) trends in the *critical* crack extension load with crack length.

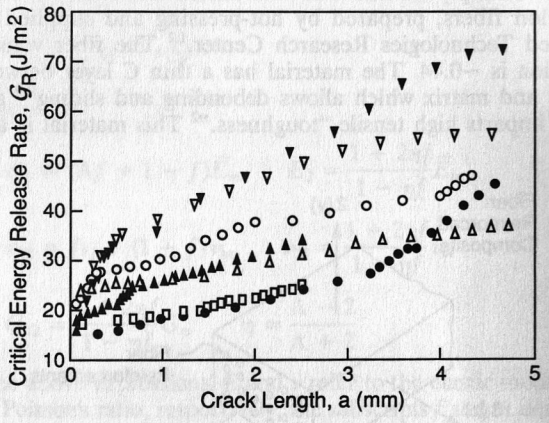

Fig. 5. Crack growth resistance curves obtained for a series of six different test specimens.

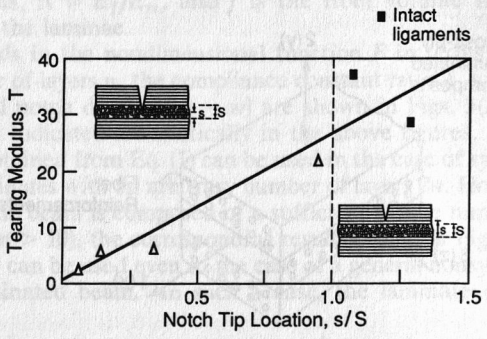

Fig. 6. Plot of trends in the tearing modulus with notch tip location. When $s/S > 1$, the notch tip is in a 0° layer and an intact bridge exists at the notch tip.

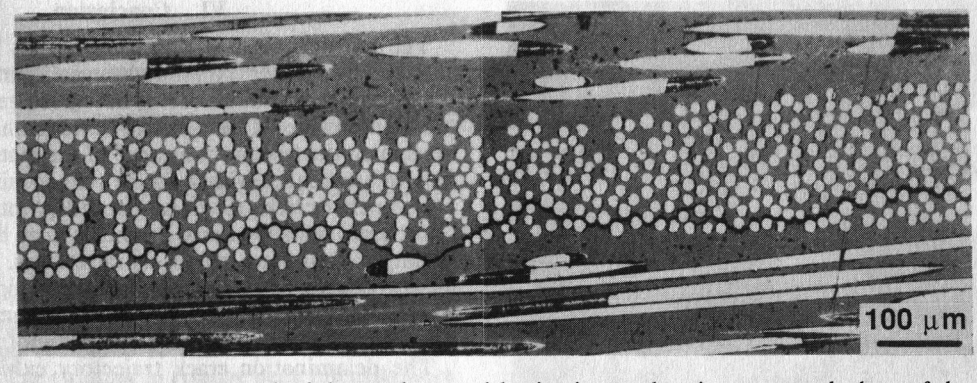

Fig. 7. Optical micrograph of the steady-state delamination crack trajectory near the base of the 90° layer.

ward the lower interface as it extended to a length $a \approx w/2$, and thereafter remained in a constant trajectory adjacent to that interface. It is important to emphasize that the steady-state crack did not select the matrix-only interlayer material, but remained just within the fiber-reinforced 90° layer (Fig. 8). Furthermore, it is noted that, when the notch tip terminates in the 0° layer, the crack nucleates *beneath* the notch, within the 90° layer (Fig. 8(C)) such that a bridge of intact material is retained between the notch tip and the delamination crack surface. But again, the crack extends into the same steady-state trajectory.

After appreciable steady-state crack extension, the crack surfaces are found to be bridged by intact fibers that distort and pull out as the crack surfaces open (Fig. 9). These fibers resist crack extension, as elaborated below.

V. Discussion

The observation that the resistance to crack growth initiation is about the same for all test specimens ($\mathcal{G}_c \approx 15$ to 20 $J \cdot m^{-2}$) indicates that a common mechanism is involved. Furthermore, the crack extends through a mix of matrix material and interface (Fig. 8) without significant fiber bridging. A first estimate of the fracture resistance is thus

$$\mathcal{G}_c \approx f\Gamma_i + (1 - f)\Gamma$$

where f is the fiber volume fraction, Γ_i is the fracture energy of the interface, and Γ_m is the fracture energy of the matrix. Prior research on these materials has suggested the values $\Gamma_m \approx 20$ to 40 $J \cdot m^{-2}$ and $\Gamma_i < 1\ J \cdot m^{-2}$.[11,12] The resulting fracture resistance $\mathcal{G}_c$, given that $f \approx 0.44$, would thus be in the

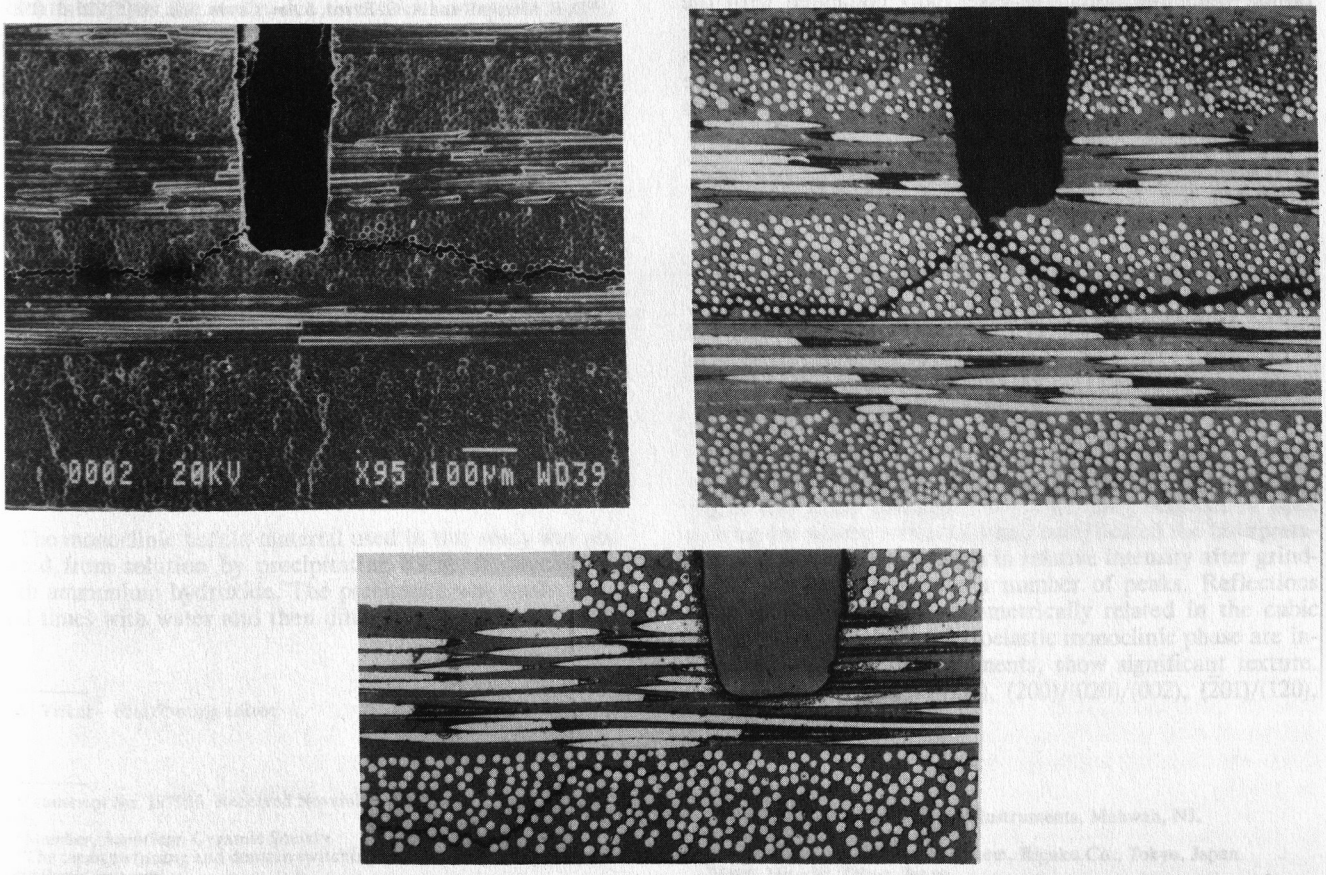

Fig. 8. Series of optical and scanning electron micrographs which reveal the initial crack trajectory toward the base of the 90° layer.

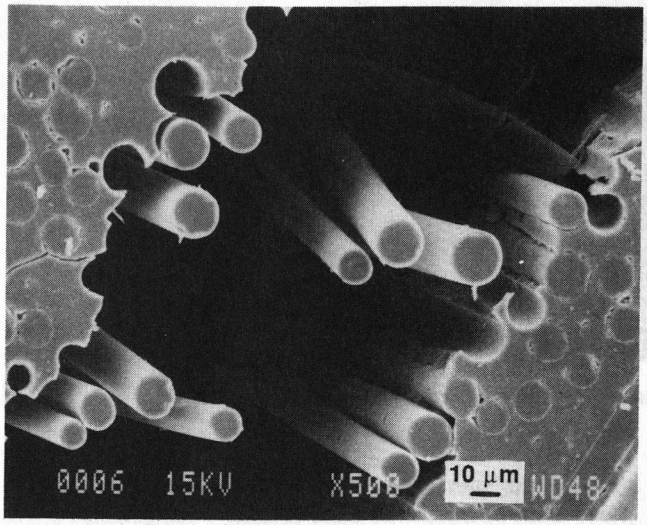

Fig. 9. Scanning electron micrograph of fibers bridging the crack surfaces.

range 12 to 24 $J \cdot m^{-2}$, which encompasses the measured range of 15 to 20 $J \cdot m^{-2}$. A reasonably consistent description of crack growth initiation thus obtains.

The dependence of the tearing modulus on *notch location* (Fig. 6) may be attributed to the ligament of bridging material between the base of the notch and the steady-state crack trajectory (Fig. 7). This ligament acts as a "hinge," which inhibits the deflection of the beam and in such cases $\mathcal{G}$ cannot be interpreted using Eq. (1). Consequently, the strictly *material-related* results are those having the smallest T, obtained when the notch tip essentially coincided with the steady-state trajectory. The associated magnitude of the tearing modulus is attributed to the tractions caused by the fibers that bridge the crack surface. Elastic spring models could be used to interpret these results,[13] including possible deviations from small-scale bridging.

VI. Conclusion

The propagation of delamination cracks has been characterized in a 0°/90° laminated ceramic-matrix composite. Crack growth resistance curves have been generated with two principal features. Crack growth initiation has been shown to depend on the fracture resistance of the matrix and the interface in accordance with a simple rule-of-mixtures law. However, further crack growth is impeded by intact fibers and, in some cases, intact matrix ligaments that bridge the crack, leading to resistance curve characteristics. Increased resistance to delamination cracking can thus be achieved by choosing a higher toughness matrix and by incorporating some fibers that thread across the delamination fracture plane.

The delamination crack trajectory exhibits steady-state characteristics whereby the crack selects a propagation plane with a 90° layer adjacent to the matrix layer between laminations. This trajectory includes matrix material and interfaces. The results of this study could be combined with analysis of resistance curves in mode I loading to interpret and predict preferred crack extension paths in laminated ceramic-matrix composites.

References

[1]K. M. Prewo, *J. Mater. Sci.*, **21**, 3590 (1986).
[2]O. Sbaizero and A. G. Evans, *J. Am. Ceram. Soc.*, **69** [6] 481–86 (1986).
[3]S. S. Wang; pp. 642–63 in ASTM Special Technical Publication, No. 674, Composite Materials: Testing and Design. Edited by S.W. Tsai. American Society for Testing and Materials, Philadelphia, PA, 1979.
[4]M. F. Ashby, E. E. Easterling, R. Harrysson, and S. K. Maiter, *Proc. R. Soc. London.*, **A398**, 261–80 (1985).
[5]Z. Suo, Harvard University Report, Mech-135; to be published in *J. Appl. Mech.*
[6]P. G. Charalambides; in Proceedings, Industry-University Advanced Materials Conference II, Denver, CO, March 1989. Advanced Materials Institute, Golden, CO, 1989.
[7]P. G. Charalambides, J. Lund, A. G. Evans, and R. M. McMeeking, *J. Appl. Mech.*, **56**, 77 (1989).
[8]J. J. Brennan and K. M. Prewo, *J. Mater. Sci.*, **17**, 2371 (1982).
[9]E. Bischoff, O. Sbaizero, M. Rühle, and A. G. Evans, *J. Am. Ceram. Soc.*, **72** [5] 741–45 (1989).
[10]D. B. Marshall and A. G. Evans, *J. Am. Ceram. Soc.*, **68** [5] 225–31 (1985).
[11]D. B. Marshall and W. Oliver, *J. Am. Ceram. Soc.*, **70** [8] 542–48 (1987).
[12]T. P. Weihs, C. M. Dick, and W. D. Nix; pp. 247–53 in MRS Proceedings, Reno, NV, March 1988, Vol. 120. Materials Research Society, Pittsburgh, PA, 1988.
[13]B. Budiansky, J. C. Amazigo and A. G. Evans, *J. Mech. Phys. Solids*, **36** 167 (1988). □